Room Temperature Anomalous Coherent Excitonic Optical Stark Effect in Metal Halide Perovskite Quantum Dots

Megha Shrivastava[1], Franziska Krieg[2,3], Dipendranath Mandal[1], Ajay K. Poonia[1], Santu K. Bera[1], Maksym V. Kovalenko[2,3], and K.V. Adarsh[1*]

[1]*Department of Physics, Indian Institute of Science Education and Research, Bhopal 462066 India*

[2]*Laboratory of Inorganic Chemistry, Department of Chemistry and Applied Biosciences, ETH Zürich, CH-8093 Zürich, Switzerland*

[3]*Empa – Swiss Federal Laboratories for Materials Science and Technology, CH-8600 Dübendorf, Switzerland*

Corresponding Author*

Email: adarsh@iiserb.ac.in

KEYWORDS. Floquet states, Biexciton, room temperature, optical Stark effect

ABSTRACT. Non-resonant optical driving of confined excitons and biexcitons in low dimensional semiconductors can open up exciting opportunities for experimentally realizing strongly interacting photon-dressed (Floquet) states through optical Stark effect (OSE) for coherent modulation of exciton state. Here, we report the first room temperature observation of Floquet biexciton mediated anomalous coherent excitonic OSE in $CsPbBr_3$ quantum dots (QDs) using circularly polarized ultrafast lasers. Remarkably, the strong exciton-biexciton interaction leads to the coherent redshift and splitting of the exciton resonance as a function of the drive photon frequency similar to Autler-Townes splitting in atomic and molecular systems. The large biexciton binding energy of 71 ± 1 meV and exciton-biexciton transition dipole moment 25 ± 1 Debye makes it possible to observe the hallmark results even at large detuning energies of more than 300 meV. This is accompanied by an unusual crossover from linear to non-linear fluence dependence of the OSE as a function of drive photon frequency. Our systematic studies in the metal halide perovskite QDs reveal crucial information on the unexplored many-body coherent interacting regime, making them suitable for room temperature quantum devices based on spin qubits.

Time-periodic optical driving is a powerful tool for manipulating quantum systems and has led to exotic quantum phases such as time crystals[1] and topological phases[2,3] that will benefit quantum metrology[4]. Of particular interest is the excitonic optical Stark effect (OSE) commonly described as the energy shift in a two-level system arising from the coherent nonlinear light-matter interactions[5–9]. This can be understood in terms of state repulsion of the photon-dressed states (Floquet states) and the original states that exist only for the coherent (pump pulse) duration. In general, the spectroscopic evidence of the OSE exhibits a blueshift of the transition energy[5,7,10–14], which increases linearly with the light intensity and inversely with the detuning energy. Multiple studies in bulk semiconductors[11] and nanostructures (0-2 dimension)[5,10,12,13,15,16] have explored the nature of spin-selective excitonic OSE for a non-resonant photoexcitation in the framework of a non-interacting exciton regime. These studies demonstrated a strong coherent signal resulting from blueshift of exciton absorption only for the same pump-probe polarization. Because of the coherent nature, OSE has many promising applications in engineering the quantum states[13,17,18] and coherent optical modulation for switching[18–20] and generating mode-locked pulses[18,21,22]. In contrast, the interacting regime of exciton–biexciton coupling leads to the phenomena that are qualitatively different from those in the non-interacting exciton framework and result in the coherent redshift of the exciton resonance. Optical Stark redshift has been observed in CuCl single crystal[23,24], monolayer transition metal dichalcogenides[17,25], InGaAs quantum wells[26], and molecular beam epitaxy grown single QDs like Mn doped CdTe[27], InGaAs/GaAs[28], and GaAs/AlGaAs[29] having appreciable exciton–biexciton coupling. Such effects are limited to only cryogenic temperatures mainly because of the low binding energies of the biexcitons which is of the order of several tens of μeV to less than several tens of meV (< 40 meV). Obviously, for many practical applications

involving quantum states of matter, it would be desirable to observe these effects at room temperature.

Metal halide perovskite (MHP) quantum dots (QDs) of the general formula ABX_3 (where A = MA/FA/Cs; B = Pb/Sn; and X = Cl/Br/I) are particularly attractive for studying the coherent light-matter interactions since in many ways they behave as a molecular system of customizable atoms like features[30–33]. The low-cost solution processability and easiness to integrate with existing nanofabrication facility make them much more attractive[34,35]. Moreover, the strong band-edge exciton-photon coupling[36], defect tolerant electronic structure of trap-free nature[34,35,37–39], discrete and narrow-bandwidth exciton transitions[5,11,39], and scalable production of highly coherent quantum emitters[37,40] make them an ideal candidate to study the coherent and spin selective light-matter interactions at room temperature. Not to mention, the multiexciton interactions in MHP QDs, particularly $CsPbBr_3$, is reasonably strong[32,41] and thus can influence the coherent light-matter interactions. Recently, we have demonstrated a spectrally well-resolved exciton and biexciton resonance in a weakly confined $CsPbBr_3$ QDs with a high binding energy ~30-40 meV for both excitons and biexcitons at room temperature[42,43]. The biexciton binding energy can further easily be tuned to higher values using quantum confinement effect (reducing the QD size)[32]. Such control over the biexciton binding energy is much more difficult in epitaxially grown QDs. In line with these expectations, OSE in MHP QDs are often overlooked by existing experimental and theoretical models[5,11,12], which question the nature of coherent exciton-exciton interactions in a two level model. Despite possessing favourable properties and being a potential candidate, a complete understanding of the coherent OSE in strongly interacting excitons framework in MHP QDs at room temperature is lacking and largely remains unexplored. Here, using solution processed strongly confined $CsPbBr_3$ QDs ~ 6 nm having biexciton binding energy **7**1 ± 1 meV,

we demonstrate the first room temperature experimental realization of the biexciton mediated anomalous OSE, which evolves from the energy redshift to the splitting of the exciton resonance as a function of the drive photon frequency. This is accompanied by the unusual crossover from linear to nonlinear fluence dependence of the optical Stark shift. The unusualities observed stimulated the consideration of the three-level system than just the two level system commonly employed in non-interacting framework. By constructing an extended Jaynes-Cummings model for three-level system we could account for all the main observations in our experiment. These findings reveal the strong influence of exciton-biexciton coupling on the coherent modulation of the exciton resonance in MHP QDs. Further the Rabi energy determined to be 83 ± 2 meV and corresponding exciton-biexciton transition dipole moment 25 ± 1 Debye are larger than any known systems, promoting the strong candidature of MHP QDs for exploitation in applications involving many-body coherent phenomena such as entangled photon pair generation and biexciton lasing.

Long-chain, zwitterion-capped $CsPbBr_3$ QDs were synthesized by facile hot injection method, and spin-coated onto an ITO-coated glass microscope slide for optical measurements; the details are provided in the Supporting Information. A high angle annular darkfield scanning transmission electron micrograph (HAADF-STEM) (Figure 1a) confirm the high degree of size uniformity and a cuboid morphology with an average size of 6 nm that lies in the region of strong quantum confinement. The ground-state optical absorption of the sample shown in Figure 1b demonstrates a sharp exciton peak and a continuum band. By using the Elliott model for the Wannier-Mott exciton[44,45], details in Supporting Information, we calculated the exciton resonance energy (E_0) = 2.405 ± 0.002 eV and continuum energy 2.479 ± 0.002 eV, which reveal the exciton binding energy, E_x = 74 ± 2 meV, that agrees with our temperature-dependent photoluminescence (PL) measurements discussed in the Supporting Information.

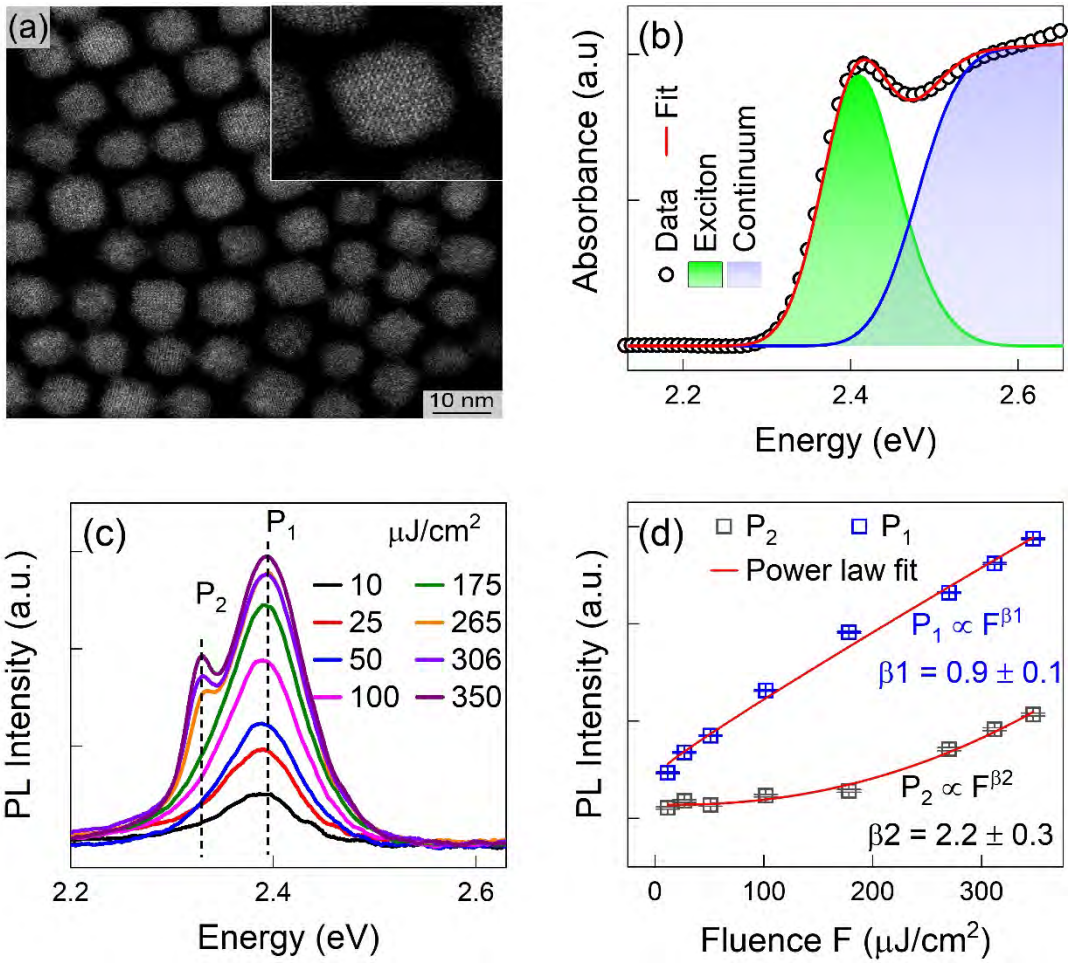

Figure 1. Morphological and optical characterization of $CsPbBr_3$ QDs. *(a) HAADF-STEM of a typical sample of ca. 6 nm $CsPbBr_3$ QDs; (b) Optical absorption spectrum fitted using the Elliott model; (c) Intensity dependent PL demonstrating exciton (P_1) and biexciton (P_2) emission; (d) Power-law fitting of P_1 (~2.39eV) and P_2 (~2.32 eV) intensity revealing a near-linear and near-quadratic intensity dependence with exponent $\beta 1$ ~0.9 and $\beta 2$ ~2.2 indicating that it is due to exciton and biexciton emission, respectively.*

To identify the biexciton states, we studied the PL under 400 nm pulsed excitation with different excitation fluences (Figure 1c), details in Supporting Information. At low excitation fluence, we observed PL from exciton emission (P_1), however, a second sharp peak (P_2) emerges towards the low energy at higher fluences. The P_1 peak exhibit a near linear fluence dependence

($I_{P1} \propto$ Fluence$^{\beta 1}$ with $\beta 1 = 0.9 \pm 0.1$) as expected from the exciton emission peak. On the other hand, the superlinear fluence dependence ($I_{P2} \propto$ Fluence$^{\beta 2}$ with $\beta 2 = 2.2 \pm 0.3$) of P_2 shown in Figure 1d reveals that it is originating from the biexciton transition[46–48]. The details are given in Supporting Information. Strikingly, above a threshold pump fluence of 175 μJ/cm^2, we observed amplified spontaneous emission kind of behaviour at the biexciton position with a reduced full-width half maximum. The biexciton binding energy E_b calculated using P_1-$P_2 = 71 \pm 1$ meV, is well in agreement with the E_b obtained from our transient absorption measurements, details in the Supporting Information. The Haynes factor, $E_b/E_x = 0.96 \pm 0.05$, is consistent with our recent report in weakly confined $CsPbBr_3$ QDs[42] and is an order of magnitude larger than the bulk and five times the 2-dimensional and quantum well semiconductors, demonstrating a very robust correlation of excitons[48–50].

We employed circularly polarized transient absorption spectroscopy to measure the interacting many-body Floquet state mediated OSE in strongly confined $CsPbBr_3$ QDs. An optical parametric amplifier generating ~120 fs broadly tunable 2.08-2.32 eV pump pulses was used to excite the sample. The resulting changes in the absorption spectrum (ΔA) were measured using a probe pulse in the photon energy range 2.30−2.55 eV. The experimental setup details are provided in the Supporting Information. To generate the coherent OSE and avoid any real population excitation, the pump photon energy was kept below E_0. Figure 2a,b show a compilation of the room temperature transient absorption spectra for σ^+pump and σ^-probe ($\sigma^+\sigma^-$) and $\sigma^+\sigma^+$ for detuning energies ($\Omega = E_0 - \hbar\omega$) 316 and 82 meV at a fixed pump pulse fluence of 1 mJ/cm^2, where $\hbar\omega$ is pump photon energy. Here, σ^+ and σ^- denote right circular and left circular polarization, respectively. The top panel presents the pseudo-color plot of the ΔA, and the bottom panel represents the cross-section close to zero pump−probe delay. The instantaneous response of the

ΔA spectrum shows that the signal is primarily originating from the coherent OSE. First, we discuss the Ω = 316 meV ΔA spectrum for $\sigma^+\sigma^-$ close to zero pump−probe delay.

The spectrum manifests a bleach at E_0 and the emergence of an induced absorption (2.40 eV) appearing below E_0, displaying a 5 meV coherent redshift of the exciton transition. We used the traditional Gaussian shifting method[43,44] to extract the Stark shift from the experimental data. Our results are compelling and show a sharp contrast with the previous studies on bulk and two-dimensional MHP films, where no signal for bulk[11] and weaker transient signal for two-dimensional MHPs[12] was observed for the $\sigma^+\sigma^-$.

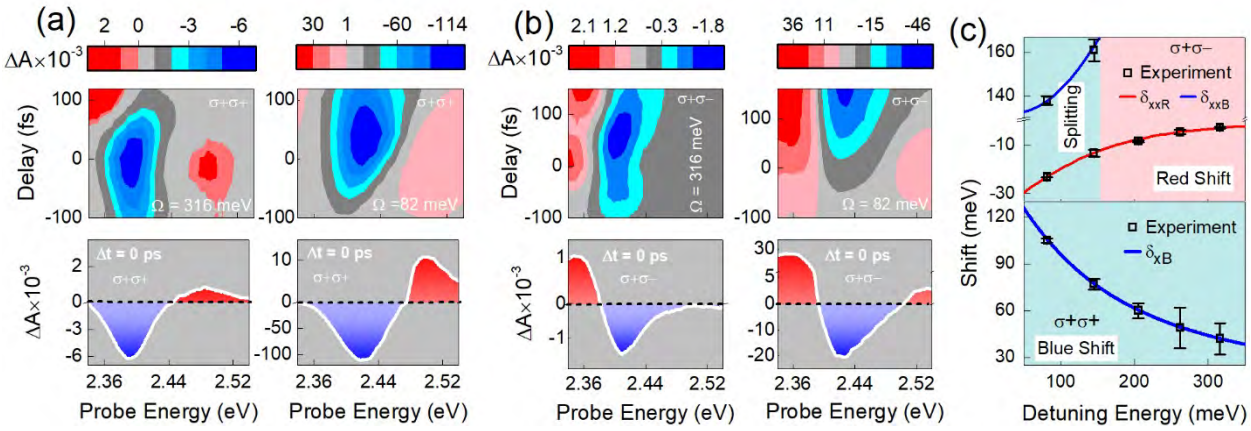

Figure 2. Anomalous excitonic OSE at fluence of 1mJ/cm^2. *Pseudo-colour plot (top) and crossection at near zero pump-probe delay (bottom) at detunings of 316 (left) and 82 meV (right) with pump fluence of 1mJ/cm^2 for (a) $\sigma^+\sigma^-$ and (b) $\sigma^+\sigma^+$. The existence of a strong signal only for the pump-pulse duration confirms the coherent response. However, at longer delays, i.e., after ~120 fs, a weak signal also exists due to the unintentional real-excitation population arising from two-photon absorption; (c) The stark shift evaluated from the experimental data (symbols) showing an excellent agreement with theoretical calculations (solid lines).*

This coherent redshift clearly demonstrates that the non-interacting exciton picture cannot fully describe the OSE in $CsPbBr_3$ QDs since they have a strong biexciton state with $E_b \approx E_x$ at room

temperature. To get further information, we have analyzed the ΔA spectrum by continuously reducing Ω from 316 to 82 meV, Figure S5 in Supporting Information. Strikingly, for Ω = 82 meV, the spectrum is dominated by the exciton energy splitting of Autler-Townes type with induced absorption at energies both above and below E_0 and a reduction of bleach at E_0 as shown in Figure 2a. This anomalous OSE of exciton shift originates from the remarkably high biexciton binding energy that embarks the observation of hallmark results even at large detuning energies of more than 300 meV, which is three orders of magnitude larger than CuCl single crystals[24], around two orders of magnitude larger than InGaAs quantum wells[26] and InGaAs/GaAs single QD[28], and four times of monolayer transition metal dichalcogenides[17]. Our experimental results demonstrate the importance of many-body interactions determining the OSE in MHP QDs.

The $\sigma^+\sigma^+$ ΔA spectrum of $CsPbBr_3$ QDs for Ω = 316 meV close to zero pump−probe delay indicates a 40 meV coherent blueshift of the exciton absorption, manifested as a reduction in E_0 and the emergence of an induced absorption at 2.445 eV (Figure 2b). The blueshift is present there for all Ω and becomes more significant as pump energy approaches exciton resonance, Figure 2b and Figure S5 in the Supporting Information, similar to the ordinary OSE previously reported in MHPs in a non-interacting exciton regime[5,11,12]. It is important to note here that despite the below bandgap excitation, we cannot discard the possibilty of the presence of real population of the carriers, since the excitation fluence is sufficiently high to cause the two photon absorption (TPA) that result in the hot carrier population in the system. The remanent signal after the coherent duration shown in Figure S6 in the Supporting Information, manifest the signal originating from TPA induced real carrier population. However, this will not affect the main result of biexciton mediated coherent OSE presented in this manuscript. The TPA will create the hot carrier population in the system, and these hot carriers will take time to travel to the band-edge and by

that time the signal originating from the coherent interactions will be over. To experimentally support our claim, we plot the amplitude of the coherent bleach in $\sigma^+\sigma^-$ at zero pump-probe delay against the fluence in the Supporting Information, Figure S7. The figure manifests the linear fluence dependence in stark contrast to the quadratic dependence expected from the TPA induced signal[12], confirming that the coherent signal is independent of TPA. To further support our argument, first, we measure the threshold fluence (> 0.5 mJ/cm^2) for TPA at $\hbar\omega$ = 2.32 eV using a conventional Z-scan and then measure the OSE below the threshold fluence (~ 0.3 mJ/cm^2), Figure S7 in Supporting Information. The Autler-Townes like splitting of the exciton resonance even at this low fluence implies that the OSE observed here is originating from the coherent interactions and not from the TPA.

To uncover further experimental facts promoting the idea of interacting exciton many-body states in the OSE of $CsPbBr_3$ QDs, we measured the optical Stark shift as a function of Ω (Figure 2c). The exciton energy redshift well defined away from the exciton–biexciton resonance for $\sigma^+\sigma^-$ evolve to an energy splitting of Autler-Townes type as Ω approaches to resonance. For $\sigma^+\sigma^+$, we did not observe any such split of the exciton resonance. Strikingly, the Autler-Townes like exciton splitting for $\sigma^+\sigma^-$ increases with increase in Ω, in stark contrast to decrease in blueshift for $\sigma^+\sigma^+$, describing the unusual OSE in terms of Ω.

To understand the mechanism behind the anomalous OSE, we took into consideration of the exciton-biexciton coherent interaction and constructed an extended Jaynes-Cummings model for three-level[51,52], as shown in Figure 3a-c, details in the Supporting Information. In the figure, $|g, n\hbar\omega\rangle$, $|x, n\hbar\omega\rangle$, $|x', n\hbar\omega\rangle$, and $|xx', n\hbar\omega\rangle$ represent bare light-matter states that account for exciton and biexciton absorption. Here $|g\rangle$, $|x\rangle$, $|x'\rangle$, and $|xx'\rangle$ represent the ground state, spin-up exciton, spin-down exciton, and biexciton, respectively. The integer n represents the number of

photons at the pump frequency ω. This three-level model, used previously to quantify coherent modulation of the quantum states in semiconductors[53–56], can easily be modified in the presence of exciton-biexciton interactions to describe the anomalous OSE in $CsPbBr_3$ QDs.

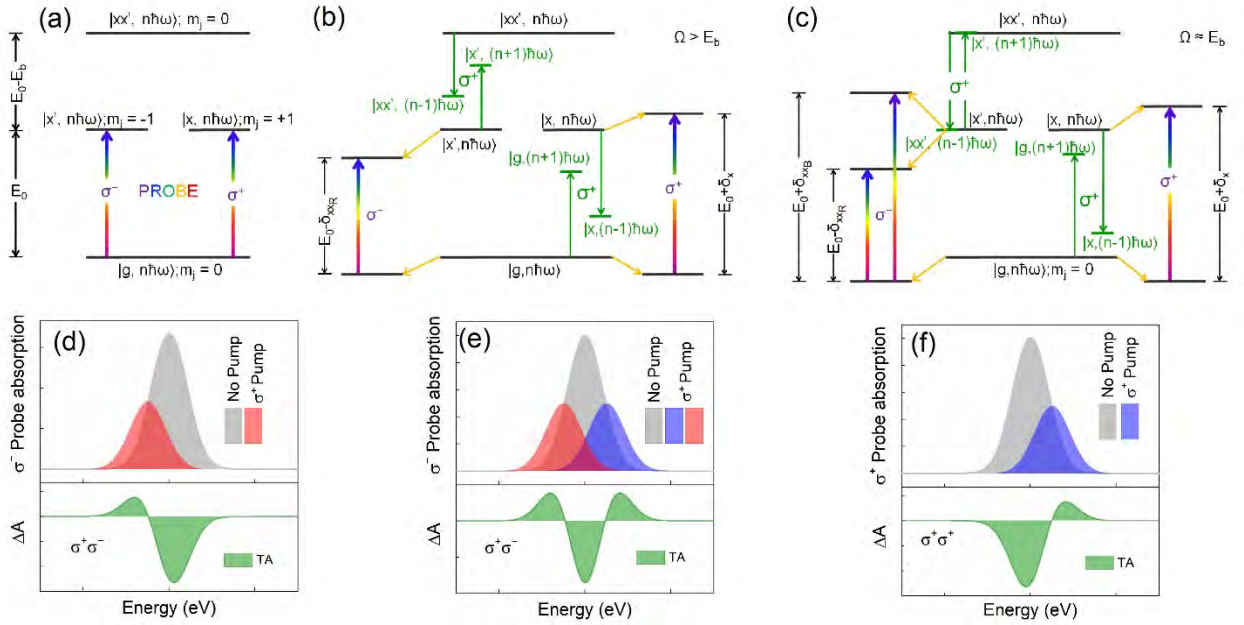

Figure 3. Three-level Jaynes-Cummings model. *(a) illustration of probe absorption in absence of pump; Floquet states (green lines) and resulting shifts under σ^+ pump for (b) $\Omega > E_b$ and (c) $\Omega \approx E_b$. The red and blue arrows represent the redshift and blueshift of the exciton resonance, respectively; (d)-(f) Illustration of coherent signal arising on (d) redshift and (e) splitting under $\sigma^+\sigma^-$, and on (f) blueshift under $\sigma^+\sigma^+$.*

In our scheme, the σ^+ probe measures the change in $|g, n\hbar\omega\rangle \rightarrow |x, n\hbar\omega\rangle$ transition, while σ^- measures the change in $|g, n\hbar\omega\rangle \rightarrow |x', n\hbar\omega\rangle$ in presence of an intense non-resonant σ^+ pump, detuned below the exciton resonance energy, producing a series of photon replicas of the original states known as the Floquet states (green lines), Figure 3a-c. Floquet states having the same m_j (magnetic quantum number) as that of original states repel each other (Figure 3b,c) giving rise to

the novel coherent features. With this idea, we first constructed the effective Hamiltonian (H) for the $\sigma^+\sigma^-$ taking $|g, n\hbar\omega\rangle$, $|x, (n-1)\hbar\omega\rangle$, $|x', n\hbar\omega\rangle$, and $|xx', (n-1)\hbar\omega\rangle$ as basis states described by

$$H = \begin{pmatrix} 0 & V_x & 0 & 0 \\ V_x & \Omega & 0 & 0 \\ 0 & 0 & E_0 & V_{xx} \\ 0 & 0 & V_{xx} & E_0 + \Omega - E_b \end{pmatrix} \quad (1)$$

Where $V_x = \mu_x E_{effective}$ and $V_{xx} = \mu_{xx} E_{effective}$ are the Rabi energies which are proportional to square root of fluence. $E_{effective}$, μ_x, and μ_{xx} describe the pump photon electric field, exciton transition dipole moment, and exciton-to-biexciton transition dipole moment, respectively. In general, $\mu_{xx} \approx \mu_x$[57] and so $V_{xx} \approx V_x$. The Eigen values of the Hamiltonian matrix represent the redshift (δ_{xx_R}) and blueshift (δ_{xx_B}) of the exciton resonance as

$$\delta_{xx_R} = \frac{\sqrt{(\Omega - E_b)^2 + 4V_{xx}{}^2}}{2} - \frac{\Omega - E_b}{2} - \frac{\sqrt{\Omega^2 + 4V_x{}^2}}{2} + \frac{\Omega}{2} \quad (2)$$

$$\delta_{xx_B} = \frac{\sqrt{(\Omega - E_b)^2 + 4V_{xx}{}^2}}{2} + \frac{\Omega - E_b}{2} + \frac{\sqrt{\Omega^2 + 4V_x{}^2}}{2} - \frac{\Omega}{2} \quad (3)$$

These equations show that the exciton–biexciton interactions dramatically modify the coherent light–matter interactions from the non-interacting exciton picture discussed in previous studies[5,11,12], and lead to a new set of optically driven coherent phenomena as a function of Ω. The detailed description is given in the Supporting Information. In particular, depending upon whether $\Omega > E_b$ or $\Omega \approx E_b$, the $|xx', (n-1)\hbar\omega\rangle$ lies above or nearly at the same level of $|x', n\hbar\omega\rangle$ (Figure 3b,c), respectively resulting in redshift or splitting of the exciton state. Noticeably, in both cases the $|x, (n-1)\hbar\omega\rangle$ lies above the $|g, n\hbar\omega\rangle$ resulting in the downshift of the ground state. The exact shift in exciton resonance is the combined shift in ground and exciton state (Equation 2 and 3), details in the Supporting Information. The schematic of coherent transient signal resulting from redshift and splitting of exciton resonance is shown in Figure 3d,e.

After demonstrating the anomalous OSE, we set up the effective Hamiltonian matrix for the $\sigma^+\sigma^+$ in the interacting exciton picture as discussed in the Supporting Information and the eigen values of the matrix correspond to the blueshifted excitonic level is given by

$$\delta_x = -\Omega + \sqrt{\Omega^2 + 4V_x{}^2} \quad (4)$$

Since the $|g, (n+1)\hbar\omega\rangle$ lies below the $|x, n\hbar\omega\rangle$ and the $|x, (n-1)\hbar\omega\rangle$ lies above the $|g, n\hbar\omega\rangle$ for $\Omega \geq E_b$ (Figure 3b,c) the repulsion between the Floquet and the original states cause the exciton resonance to blueshift by δ_x. The illustration of the coherent signal resulting from blueshift of exciton resonance is shown in Figure 3f. There is no contribution from the biexciton interaction in $\sigma^+\sigma^+$, the theoretical description is exactly the same as that of the ordinary OSE in a non-interacting framework[10,12,58].

To make a quantitative comparison between experiment and theory in the interacting regime, we numerically simulated the spectrum at different Ω by solving the effective Hamiltonian in Equation 1 and Supporting Information. The simulation is accomplished by using homogeneous broadening of 100 meV and biexciton binding energy of 71 meV. The Rabi energy extracted is $V_{xx} \approx V_x = 83 \pm 2$ meV and corresponding $\mu_{xx} \approx \mu_x = 25 \pm 1$ Debye. The biexciton transition dipole moment is larger than those of any known systems, such as CuCl (~20 Debye), monolayer $MoSe_2$ (9.3 Debye), and GaAs/AlGaAs quantum dot (10 Debye)[17,24,29]. Figure 4a shows that calculated ΔA spectrum of $\sigma^+\sigma^-$ for a pump fluence of 1 mJ/cm^2, presented as pseudo-color plot, at different detuning energies reasonably matches with the experimental ΔA spectrum. Moreover, the blueshift and redshift for the $\sigma^+\sigma^-$ and blueshift in $\sigma^+\sigma^+$, is exactly matching with our theoretical calculations, solid lines in Figure 2c.

The other prominent signature of strong coherent exciton-biexciton interactions is obtained from the fluence-dependent ΔA for $\sigma^+\sigma^-$ and $\sigma^+\sigma^+$. Similar to detuning energy dependence, the

Jaynes-Cummings model can be employed to account for the fluence dependence as well. For instance, the pseudo-color plots in Figure 4b demonstrates the excellent agreement between experimentally and theoretically calculated ΔA spectra ($\sigma^+\sigma^-$) at different pump-fluences for Ω = 82 meV.

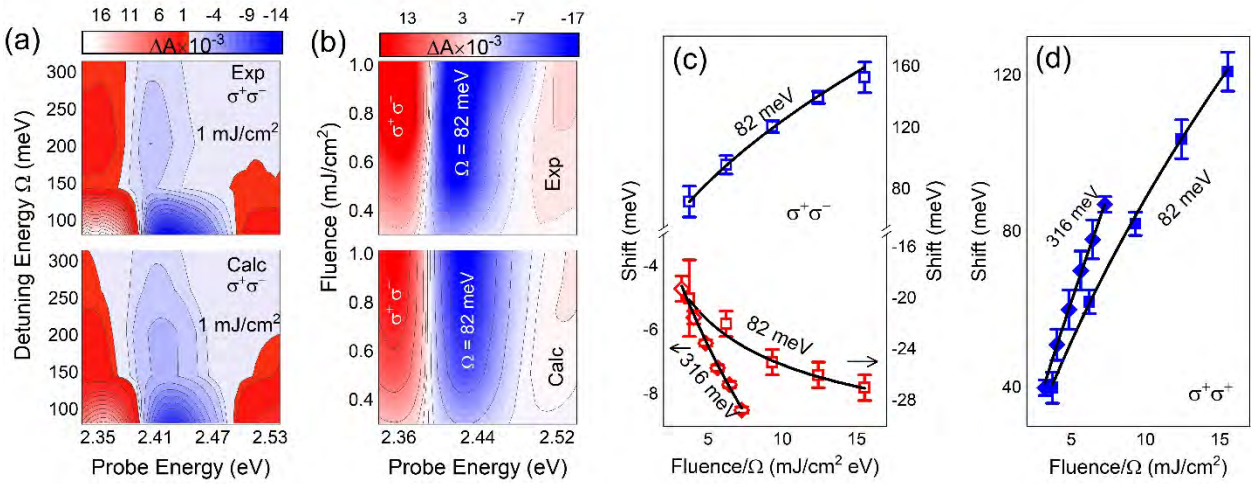

Figure 4. Detuning and fluence dependent OSE. *Pseudo-colour plot of the experimental (top) and theoretically calculated (bottom) ΔA at zero pump-probe delay as a function of (a) Ω at constant fluence of 1mJ/cm^2 and of (b) fluence at constant Ω = 82 meV, under $\sigma^+\sigma^-$; The optical stark shift evaluated experimentally (symbols) and theoretically calculated (solid lines) at different fluences at Ω = 316 meV and 82 meV for (c) $\sigma^+\sigma^-$ and (d) $\sigma^+\sigma^+$.*

The optical Stark shift evaluated at different fluences at two extreme Ω used in present study, 316 and 82 meV, is shown in Figure 4c for $\sigma^+\sigma^-$ and Figure 4d for $\sigma^+\sigma^+$. Under Ω = 316 meV, the optical stark shift for $\sigma^+\sigma^-$ (hollow red diamond) and $\sigma^+\sigma^+$ (solid blue diamond) show a linear fluence dependence, which can be retrieved by including large detuning approximation ($\Omega >> V_x$) to Equation 2 and 4, that reduces to

$$\delta_{xx_R} = \frac{{V_{xx}}^2}{|\Omega| - E_b} - \frac{{V_x}^2}{|\Omega|} \quad and \quad \delta_{x_B} = \frac{2{V_x}^2}{|\Omega|} \tag{5}$$

This picture changes dramatically for Ω = 82 meV. Here, the optical Stark redshift (hollow red square) and blueshift (hollow blue square) for $\sigma^+\sigma^-$ and blueshift (solid blue square) for $\sigma^+\sigma^+$ exhibit a non-linear fluence dependence in accordance with Equation 2-4, as shown in Figure 4c,d, in stark contrast to the previous reports in two-dimensional[12] and bulk perovskites[11].

In summary, we have demonstrated the first observation of anomalous excitonic OSE at room temperature in solution processed $CsPbBr_3$ QDs that necessitate the consideration of the biexciton interactions for a complete description. Further, we anticipate that these types of coherent biexciton states can offer a pathway to explore solution processed QDs based room temperature quantum information processing, lasing, mode-locking, electromagnetically induced transparency, and to generate a pulse of light containing many photons in a highly entangled state for which the polarization state of each photon is intricately linked to others − a new resource for distributed quantum technologies.

ASSOCIATED CONTENT

Supporting Information. Synthesis of $CsPbBr_3$ QDs, circularly polarized transient absorption spectroscopy, determination of exciton binding energy through Elliott model and temperature dependent PL, Biexciton binding energy determination through fluence dependent PL and transient absorption measurements, detuning dependent OSE, time evolution of features, and theoretical description in interacting framework.

AUTHOR INFORMATION

Corresponding Author:

K. V. Adarsh - Department of Physics, Indian Institute of Science Education and Research, Bhopal 462066 India.

Phone:+91-755-2691207

E-mail: adarsh@iiserb.ac.in

Notes

The authors declare no competing financial interest.

ACKNOWLEDGEMENTS

The authors gratefully acknowledge the Science and Engineering Research Board (project no.CRG/2019/002808), DAE BRNS (sanction no. 37(3)/14/26/2016-BRNS/37245), and FIST Project for Department of Physics. M.V.K. acknowledges financial support from the European Union through Horizon 2020 research and innovation programme (ERC Consolidator Grant SCALE-HALO, Grant Agreement No. 819740). Authors acknowledge Dr. Frank Krumeich for High angle annular darkfield scanning transmission electron micrograph images collection.

REFERENCE

(1) Wilczek, F. Quantum Time Crystals. PRL 2012, 109, 160401. DOI: 10.1103/PhysRevLett.109.160401.

(2) Shtanko, O.; Movassagh, R. Stability of Periodically Driven Topological Phases against Disorder. Phys. Rev. Lett. 2018, 121, 126803. DOI: 10.1103/PhysRevLett.121.126803.

(3) Mahmood, F.; Chan, C. K.; Alpichshev, Z.; Gardner, D.; Lee, Y.; Lee, P. A.; Gedik, N. Selective Scattering between Floquet-Bloch and Volkov States in a Topological Insulator. Nat. Phys. 2016, 12, 306–310. DOI: 10.1038/nphys3609.

(4) Pang, S.; Jordan, A. N. Optimal Adaptive Control for Quantum Metrology with Time-Dependent Hamiltonians. Nat. Commun. 2017, 8, 14695. DOI: 10.1038/ncomms14695.

(5) Li, Y.; He, S.; Luo, X.; Lu, X.; Wu, K. Strong Spin-Selective Optical Stark Effect in Lead Halide Perovskite Quantum Dots. J. Phys. Chem. Lett. 2020, 11, 3594–3600. DOI: 10.1021/acs.jpclett.0c00879.

(6) Tuorila, J.; Silveri, M.; Sillanpää, M.; Thuneberg, E.; Makhlin, Y.; Hakonen, P. Stark Effect and Generalized Bloch-Siegert Shift in a Strongly Driven Two-Level System. Phys. Rev. Lett. 2010, 105, 257003. DOI: 10.1103/PhysRevLett.105.257003.

(7) Sie, E. J.; Lui, C. H.; Lee, Y. H.; Fu, L.; Kong, J.; Gedik, N. Large, Valley-Exclusive Bloch-Siegert Shift in Monolayer WS2. Science 2017, 355, 1066–1069. DOI: 10.1126/science.aal2241.

(8) Sim, S.; Lee, D.; Lee, J.; Bae, H.; Noh, M.; Cha, S.; Jo, M. H.; Lee, K.; Choi, H. Light Polarization-Controlled Conversion of Ultrafast Coherent-Incoherent Exciton Dynamics in Few-Layer ReS2. Nano Lett. 2019, 19, 7464–7469. DOI: 10.1021/acs.nanolett.9b03173.

(9) Makkar, M.; Dheer, L.; Singh, A.; Moretti, L.; Maiuri, M.; Ghosh, S.; Cerullo, G.; Waghmare, U. V; Viswanatha, R. Magneto-Optical Stark Effect in Fe-Doped CdS Nanocrystals. Nano Lett. 2021, 21, 3798−3804. DOI: 10.1021/acs.nanolett.1c00126.

(10) Sie, E. J.; McLver, J. W.; Lee, Y. H.; Fu, L.; Kong, J.; Gedik, N. Valley-Selective Optical Stark Effect in Monolayer WS2. Nat. Mater. 2015, 14, 290–294. DOI: 10.1038/nmat4156.

(11) Yang, Y.; Yang, M.; Zhu, K.; Johnson, J. C.; Berry, J. J.; Van De Lagemaat, J.; Beard, M. C. Large Polarization-Dependent Exciton Optical Stark Effect in Lead Iodide Perovskites. Nat. Commun. 2016, 7, 12613. DOI: 10.1038/ncomms12613.

(12) Giovanni, D.; Chong, W. K.; Dewi, H. A.; Thirumal, K.; Neogi, I.; Ramesh, R.; Mhaisalkar, S.; Mathews, N.; Sum, T. C. Tunable Room-Temperature Spin-Selective Optical Stark Effect in Solution-Processed Layered Halide Perovskites. Sci. Adv. 2016, 2, 1600477. DOI: 10.1126/sciadv.1600477.

(13) Von Lehmen, A.; Chemla, D. S.; Heritage, J. P.; Zucker, J. E. Optical Stark Effect on Excitons in GaAs Quantum Wells. Opt. Lett. 1986, 11, 609-611. DOI: 10.1364/OL.11.000609.

(14) Diroll, B. T. Circularly Polarized Optical Stark Effect in CdSe Colloidal Quantum Wells. Nano Lett. 2020, 20, 7889-7895. DOI: 10.1021/acs.nanolett.0c02409.

(15) Unold, T.; Mueller, K.; Lienau, C.; Elsaesser, T.; Wieck, A. D. Optical Stark Effect in a Quantum Dot: Ultrafast Control of Single Exciton Polarizations. Phys. Rev. Lett. 2004, 92, 157401. DOI: 10.1103/PhysRevLett.92.157401.

(16) Song, D.; Wang, F.; Dukovic, G.; Zheng, M.; Semke, E. D.; Brus, L. E.; Heinz, T. F. Measurement of the Optical Stark Effect in Semiconducting Carbon Nanotubes. Appl. Phys. A 2009, 96, 283–287. DOI: 10.1007/s00339-009-5202-6.

(17) Yong, C. K.; Horng, J.; Shen, Y.; Cai, H.; Wang, A.; Yang, C. S.; Lin, C. K.; Zhao, S.; Watanabe, K.; Taniguchi, T.; Tongay, S.; Wang, F. Biexcitonic Optical Stark Effects in Monolayer Molybdenum Diselenide. Nat. Phys. 2018, 14, 1092-1096, DOI: 10.1038/s41567-018-0216-7.

(18) Yumoto, G.; Hirori, H.; Sekiguchi, F.; Sato, R.; Saruyama, M.; Teranishi, T.; Kanemitsu, Y. Strong Spin-Orbit Coupling Inducing Autler-Townes Effect in Lead Halide Perovskite Nanocrystals. Nat. Commun. 2021, 12, 3026. DOI: 10.1038/s41467-021-23291-w.
(19) Mysyrowicz, A.; Hulin, D.; Antonetti, A.; Migus, A.; Masselink, W. T.; Morkoç, H. "Dressed Excitons" in a Multiple-Quantum-Well Structure: Evidence for an Optical Stark Effect with Femtosecond Response Time. Phys. Rev. Lett. 1986, 56, 2748. DOI: 10.1103/PhysRevLett.56.2748.
(20) Sim, S.; Lee, D.; Noh, M.; Cha, S.; Soh, C. H.; Sung, J. H.; Jo, M. H.; Choi, H. Selectively Tunable Optical Stark Effect of Anisotropic Excitons in Atomically Thin ReS2. Nat. Commun. 2016 , 7, 13569. DOI: 10.1038/ncomms13569.
(21) Quarterman, A. H.; Wilcox, K. G.; Apostolopoulos, V.; Mihoubi, Z.; Elsmere, S. P.; Farrer, I.; Ritchie, D. A.; Tropper, A. A Passively Mode-Locked External-Cavity Semiconductor Laser Emitting 60-Fs Pulses. Nat. Photonics 2009, 3, 729–731. DOI: 10.1038/nphoton.2009.216.
(22) Quarterman, A.; Tropper, A.; Ritchie, D. A.; Daniell, G. J.; Farrer, I.; Wilcox, K. G.; Elsmere, S.; Mihoubi, Z. Ultrafast Optical Stark Mode-Locked Semiconductor Laser. Opt. Lett. 2008, 33, 2797-2799. DOI: 10.1364/OL.33.002797.
(23) Hulin, D.; Joffre, M. Excitonic Optical Stark Redshift: The Biexciton Signature. Phys. Rev. Lett. 1990, 65, 3425. DOI: 10.1103/PhysRevLett.65.3425.
(24) Shimano, R.; Kuwata-Gonokami, M. Observation of Autler-Townes Splitting of Biexcitons in CuCl. Phys. Rev. Lett. 1994, 72, 530. DOI: 10.1103/PhysRevLett.72.530.
(25) Sie, E. J.; Lui, C. H.; Lee, Y.-H.; Kong, J.; Gedik, N. Observation of Intervalley Biexcitonic Optical Stark Effect in Monolayer WS2. Nano Lett. 2016, 16, 7421–7426. DOI: 10.1021/acs.nanolett.6b02998.
(26) Sieh, C.; Meier, T.; Jahnke, F.; Knorr, A.; Koch, S. W.; Brick, P.; Hübner, M.; Ell, C.; Prineas, J.; Khitrova, G.; Gibbs, H. M. Coulomb Memory Signatures in the Excitonic Optical Stark Effect. Phys. Rev. Lett. 1999, 82, 3112. DOI: 10.1103/PhysRevLett.82.3112.
(27) Le Gall, C.; Brunetti, A.; Boukari, H.; Besombes, L. Optical Stark Effect and Dressed Exciton States in a Mn-Doped CdTe Quantum Dot. Phys. Rev. Lett. 2011, 107, 057401. DOI: 10.1103/PhysRevLett.107.057401.
(28) Boyle, S. J.; Ramsay, A. J.; Fox, A. M.; Skolnick, M. S.; Heberle, A. P.; Hopkinson, M. Beating of Exciton-Dressed States in a Single Semiconductor InGaAs/GaAs Quantum Dot. Phys. Rev. Lett. 2009, 102, 207401. DOI: 10.1103/PhysRevLett.102.207401.
(29) Kasprzak, J.; Portolan, S.; Rastelli, A.; Wang, L.; Plumhof, J. D.; Schmidt, O. G.; Langbein, W. Vectorial Nonlinear Coherent Response of a Strongly Confined Exciton-Biexciton System. New J. Phys. 2013, 15, 055006, DOI: 10.1088/1367-2630/15/5/055006
(30) Wei, K.; Xu, Z.; Chen, R.; Zheng, X.; Cheng, X.; Jiang, T. Temperature-Dependent Excitonic Photoluminescence Excited by Two-Photon Absorption in Perovskite $CsPbBr_3$ Quantum Dots. Opt. Lett. 2016, 41, 3821-3824. DOI: 10.1364/ol.41.003821.
(31) Chen, J.; Zhang, Q.; Shi, J.; Zhang, S.; Du, W.; Mi, Y.; Shang, Q.; Liu, P.; Sui, X.; Wu, X.; Wang, R.; Peng, B.; Zhong, H.; Xing, G.; Qiu, X.; Sum, T. C.; Liu, X. Room Temperature Continuous-Wave Excited Biexciton Emission in Perovskite Nanoplatelets via Plasmonic Nonlinear Fano Resonance. Commun. Phys. 2019, 2, 80. DOI: 10.1038/s42005-019-0178-9.
(32) Castañeda, J. A.; Nagamine, G.; Yassitepe, E.; Bonato, L. G.; Voznyy, O.; Hoogland, S.; Nogueira, A. F.; Sargent, E. H.; Cruz, C. H. B.; Padilha, L. A. Efficient Biexciton Interaction in Perovskite Quantum Dots under Weak and Strong Confinement. ACS Nano 2016, 10, 8603–8609. DOI: 10.1021/acsnano.6b03908.

(33) Bera, S.; Pradhan, N. Perovskite Nanocrystal Heterostructures: Synthesis, Optical Properties, and Applications. ACS Energy Lett. 2020, 5, 2858–2872. DOI: 10.1021/acsenergylett.0c01449.
(34) Akkerman, Q. A.; Rainò, G.; Kovalenko, M. V.; Manna, L. Genesis, Challenges and Opportunities for Colloidal Lead Halide Perovskite Nanocrystals. Nat. Mater. 2018, 17, 394–405. DOI: 10.1038/s41563-018-0018-4.
(35) Kovalenko, M. V.; Protesescu, L.; Bodnarchuk, M. I. Properties and Potential Optoelectronic Applications of Lead Halide Perovskite Nanocrystals. Science 2017, 358, 745–750. DOI: 10.1126/science.aam7093.
(36) Du, W.; Zhang, S.; Zhang, Q.; Liu, X. Recent Progress of Strong Exciton – Photon Coupling in Lead Halide Perovskites. Adv. Mater. 2018, 31, 1804894. DOI: 10.1002/adma.201804894.
(37) Dey, A.; Ye, J.; De, A.; Debroye, E.; Ha, S. K.; Bladt, E.; Kshirsagar, A. S.; Wang, Z.; Yin, J.; Wang, Y.; Quan, L. N.; Yan, F.; Gao, M.; Li, X.; Shamsi, J.; Debnath, T.; Cao, M.; Scheel, M. A.; Kumar, S.; Steele, J. A.; Gerhard, M.; Chouhan, L.; Xu, K.; Wu, X. G.; Li, Y.; Zhang, Y.; Dutta, A.; Han, C.; Vincon, I.; Rogach, A. L.; Nag, A.; Samanta, A.; Korgel, B. A.; Shih, C. J.; Gamelin, D. R.; Son, D. H.; Zeng, H.; Zhong, H.; Sun, H.; Demir, H. V.; Scheblykin, I. G.; Mora-Seró, I.; Stolarczyk, J. K.; Zhang, J. Z.; Feldmann, J.; Hofkens, J.; Luther, J. M.; Pérez-Prieto, J.; Li, L.; Manna, L.; Bodnarchuk, M. I.; Kovalenko, M. V.; Roeffaers, M. B. J.; Pradhan, N.; Mohammed, O. F.; Bakr, O. M.; Yang, P.; Müller-Buschbaum, P.; Kamat, P. V.; Bao, Q.; Zhang, Q.; Krahne, R.; Galian, R. E.; Stranks, S. D.; Bals, S.; Biju, V.; Tisdale, W. A.; Yan, Y.; Hoye, R. L. Z.; Polavarapu, L. State of the Art and Prospects for Halide Perovskite Nanocrystals. ACS Nano 2021, 15, 10775–10981. DOI: 10.1021/acsnano.0c08903.
(38) Seiler, H.; Palato, S.; Sonnichsen, C.; Baker, H.; Socie, E.; Strandell, D. P.; Kambhampati, P. Two-Dimensional Electronic Spectroscopy Reveals Liquid-like Lineshape Dynamics in CsPbI3 Perovskite Nanocrystals. Nat. Commun. 2019, 10, 4962. DOI: 10.1038/s41467-019-12830-1
(39) Shrivastava, M.; Bodnarchuk, M. I.; Hazarika, A.; Luther, J. M.; Beard, M. C.; Kovalenko, M. V.; Adarsh, K. V. Polaron and Spin Dynamics in Organic–Inorganic Lead Halide Perovskite Nanocrystals. Adv. Opt. Mater. 2020, 2001016. DOI: 10.1002/adom.202001016.
(40) Utzat, H.; Sun, W.; Kaplan, A. E. K.; Krieg, F.; Ginterseder, M.; Spokoyny, B.; Klein, N. D.; Shulenberger, K. E.; Perkinson, C. F.; Kovalenko, M. V.; Bawendi, M. G. Coherent Single-Photon Emission from Colloidal Lead Halide Perovskite Quantum Dots. Science 2019, 363, 1068–1072. DOI: 10.1126/science.aau7392.
(41) Makarov, N. S.; Guo, S.; Isaienko, O.; Liu, W.; Robel, I.; Klimov, V. I. Spectral and Dynamical Properties of Single Excitons, Biexcitons, and Trions in Cesium–Lead-Halide Perovskite Quantum Dots. Nano Lett. 2016, 16, 2349–2362. DOI: 10.1021/acs.nanolett.5b05077.
(42) Poonia, A. K.; Shrivastava, M.; Mir, W. J.; Aneesh, J.; Nag, A.; Adarsh, K. V. Intervalley Polaronic Biexcitons in Metal Halide Perovskite Quantum Dots. Phys. Rev. B 2021, 104, L161407. DOI: 10.1103/PhysRevB.104.L161407.
(43) Aneesh, J.; Swarnkar, A.; Kumar Ravi, V.; Sharma, R.; Nag, A.; Adarsh, K. V. Ultrafast Exciton Dynamics in Colloidal CsPbBr 3 Perovskite Nanocrystals: Biexciton Effect and Auger Recombination. J. Phys. Chem. C 2017, 121, 4734–4739. DOI: 10.1021/acs.jpcc.7b00762.
(44) Mondal, A.; Aneesh, J.; Kumar Ravi, V.; Sharma, R.; Mir, W. J.; Beard, M. C.; Nag, A.; Adarsh, K. V. Ultrafast Exciton Many-Body Interactions and Hot-Phonon Bottleneck in Colloidal Cesium Lead Halide Perovskite Nanocrystals. Phys. Rev. B 2018, 98, 115418. DOI: 10.1103/PhysRevB.98.115418.
(45) Elliott, R. J. Intensity of Optical Absorption by Excitons. Phys. Rev. 1957, 108, 1384. DOI: 10.1103/PhysRev.108.1384.

(46) Phillips, R. T.; Lovering, D. J.; Denton, G. J.; Smith, G. W. Biexciton Creation and Recombination in a GaAs Quantum Well. Phys. Rev. B 1992, 45, 4308. DOI: 10.1103/PhysRevB.45.4308.
(47) Booker, E. P.; Price, M. B.; Budden, P. J.; Abolins, H.; del Valle-Inclan Redondo, Y.; Eyre, L.; Nasrallah, I.; Phillips, R. T.; Friend, R. H.; Deschler, F.; Greenham, N. C. Vertical Cavity Biexciton Lasing in 2D Dodecylammonium Lead Iodide Perovskites. Adv. Opt. Mater. 2018, 6, 1800616. DOI: 10.1002/adom.201800616.
(48) You, Y.; Zhang, X. X.; Berkelbach, T. C.; Hybertsen, M. S.; Reichman, D. R.; Heinz, T. F. Observation of Biexcitons in Monolayer WSe2. Nat. Phys. 2015, 11, 477–481. DOI: 10.1038/nphys3324.
(49) Birkedal, D.; Singh, J.; Lyssenko, V. G.; Erland, J.; Hvam, J. M. Binding of Quasi-Two-Dimensional Biexcitons. Phys. Rev. Lett. 1996, 76, 672. DOI: 10.1103/PhysRevLett.76.672.
(50) Singh, J.; Birkedal, D.; Lyssenko, V. G.; Hvam, J. M. Binding Energy of Two-Dimensional Biexcitons; Phys. Rev. Lett. 1996, 53,15909.
(51) Kira, M.; Koch, S. W. Semiconductor Quantum Optics; Cambridge University Press, 2011; Vol. 9780521875097. DOI: 10.1017/CBO9781139016926.
(52) Jaynes, E. T.; Cummings, F. W. Comparison of Quantum and Semiclassical Radiation Theories with Application to the Beam Maser. Proc. IEEE 1963, 51, 89–109. DOI: 10.1109/PROC.1963.1664.
(53) Ajiki, H.; Ishihara, H. Biexcitonic Cavity Quantum Electrodynamics Effect on Nonlinear Spectra of a Quantum Dot. J. Appl. Phys. 2008, 104, 123105. DOI: 10.1063/1.3043627.
(54) Torosov, B. T.; Longhi, S.; Della Valle, G. Mixed Rabi Jaynes–Cummings Model of a Three-Level Atom Interacting with Two Quantized Fields. Opt. Commun. 2015, 346, 110–114. DOI: 10.1016/j.optcom.2015.02.035.
(55) Cook, R. J.; Kimble, H. J. Possibility of Direct Observation of Quantum Jumps. Phys. Rev. Lett. 1985, 54, 1023. DOI: 10.1103/PhysRevLett.54.1023.
(56) Brewer, R. G.; Hahn, E. L. Coherent Two-Photon Processes: Transient and Steady-State Cases. Phys. Rev. A 1975, 11, 1641. DOI: 10.1103/PhysRevA.11.1641.
(57) Stievater, T. H.; Li, X.; Steel, D. G.; Gammon, D.; Katzer, D. S.; Park, D. Transient Nonlinear Spectroscopy of Excitons and Biexcitons in Single Quantum Dots. Phys. Rev. B 2002, 65, 205319. DOI: 10.1103/PhysRevB.65.205319.
(58) Cunningham, P. D.; Hanbicki, A. T.; Reinecke, T. L.; McCreary, K. M.; Jonker, B. T. Resonant Optical Stark Effect in Monolayer WS2. Nat. Commun. 2019, 10, 5539. DOI: 10.1038/s41467-019-13501-x.

TABLE OF CONTENT GRAPHIC

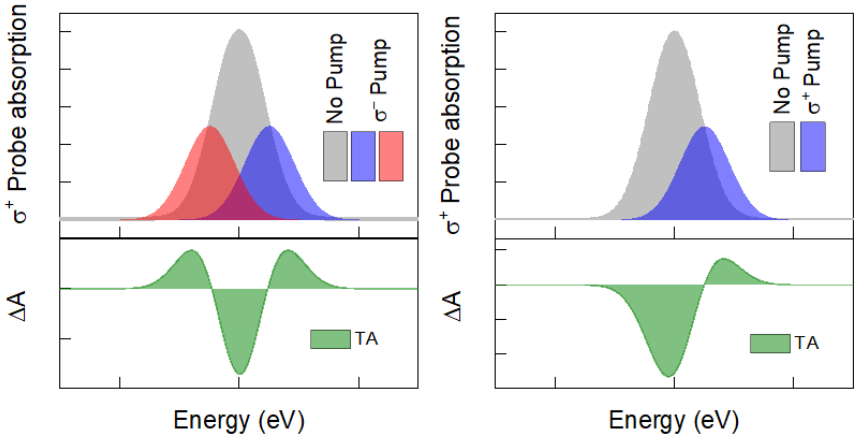

Correction:

Room-Temperature Anomalous Coherent Excitonic Optical Stark Effect in Metal Halide Perovskite Quantum Dots

Megha Shrivastava[1], Franziska Krieg[2,3], Dipendranath Mandal[1], Ajay K. Poonia[1], Santu K. Bera[1], Maksym V. Kovalenko[2,3], and K.V. Adarsh[1*]

[1]*Department of Physics, Indian Institute of Science Education and Research, Bhopal 462066 India*

[2]*Laboratory of Inorganic Chemistry, Department of Chemistry and Applied Biosciences, ETH Zürich, CH-8093 Zürich, Switzerland*

[3]*Empa – Swiss Federal Laboratories for Materials Science and Technology, CH-8600 Dübendorf, Switzerland*

Corresponding Author*

Email: adarsh@iiserb.ac.in

Nano Lett. 2022, 22, 2, 808-814. DOI: https://doi.org/10.1021/acs.nanolett.1c04471

The panel (a) and (b) of Figure 2 of this article were inadvertently swapped during production of final files. The correct version of the figure appears below.

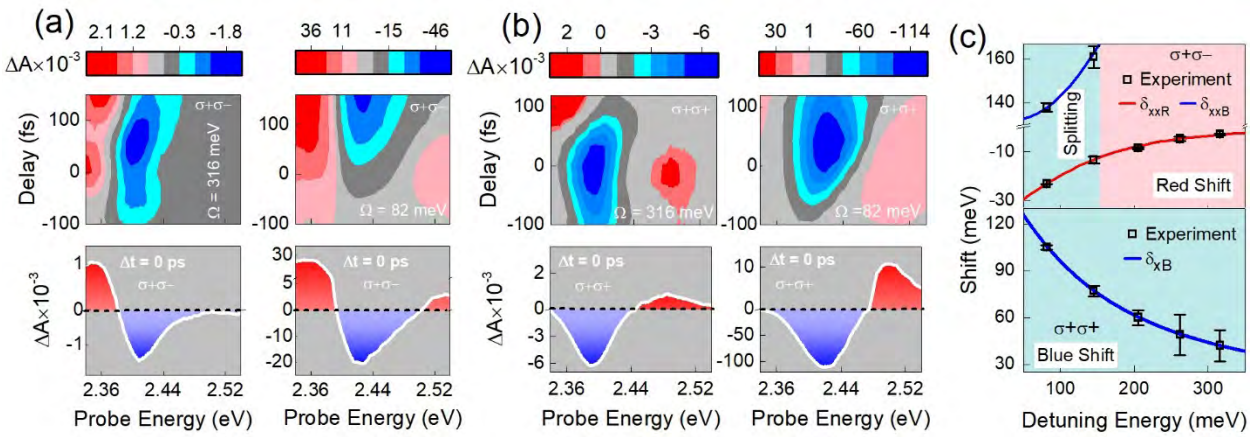
(a)
2.1 1.2 -0.3 -1.8
36 11 -15 -46
ΔA×10-3
Delay (fs)
σ+σ−
Ω = 316 meV
Ω = 82 meV
Δt = 0 ps
Probe Energy (eV)
(b)
2 0 -3 -6
30 1 -60 -114
σ+σ+
Ω = 316 meV
Ω =82 meV
(c)
Experiment
δxxR
δxxB
Splitting
Red Shift
Blue Shift
Shift (meV)
Detuning Energy (meV)